Supporting Information

Ultra-Broadband, and Ultra-high Electromagnetic Interference Shielding Performance of Aligned and Compact MXene Films

Weiqiang Huang[1#], Xuebin Liu[1#], Yunfan Wang[1], Jiyong Feng[1], Junhua Huang[1], Zhenxi Dai[1], Shaodian Yang[1,2], Songfeng Pei[3,4], Jing Zhong[5], and Xuchun Gui[*1]

[1]*State Key Laboratory of Optoelectronic Materials and Technologies, School of Electronics and Information Technology, Sun Yat-sen University, Guangzhou 510275, Guangdong, China*

[2]*National Key Laboratory of Materials for Integrated Circuits, Shenzhen Institute of Advanced Electronic Materials, Shenzhen Institute of Advanced Technology, Chinese Academy of Sciences, Shenzhen 518055, China*

[3]*Shenyang National Laboratory for Materials Science, Institute of Metal Research, Chinese Academy of Sciences, 72 Wenhua Road, Shenyang 110016, P. R. China*

[4]*School of Materials Science and Engineering, University of Science and Technology of China, 72 Wenhua Road, Shenyang 110016, P. R. China*

[5]*Key Lab of Structure Dynamic Behavior and Control (Harbin Institute of Technology), Ministry of Education, Harbin, 150090, Heilongjiang, China*

[#] *These authors contributed equally.*

*To whom correspondence. E-mail: *guixch@mail.sysu.edu.cn*

Supporting Method S1. Theoretical calculation of the centrifugal force.

The numerical value of the relative centrifugal force is determined using the following formula [1]:

$$G = \frac{R \times \omega^2}{g} = \frac{R \times \pi^2 \times S^2}{g \times 30^2} \tag{1}$$

Where G is the relative centrifugal force (denoted in units of gravitational acceleration, g), g is the gravitational acceleration (m s^{-2}), R is the centrifugal radius (m), ω is the angular velocity (rad s^{-1}), and S is the rotating rate (rpm). The specific data of relative centrifugal force are presented as follows in the table.

Centrifugal radius (m),	Rotating rate (rpm)	Relative centrifugal force (g)
0.1	1000	112
	1500	252
	2000	447
	2500	699
	3000	1006

Supporting Method S2. WAXS and theoretical calculation of Herman's orientation factor.

Wide-Angle X-ray Scattering (WAXS) tests are conducted on the Anton Paar SAXSpoint5.0 System using an incident Cu-Kα X-ray beam parallel to the film plane and striking on the cross-section of the film. The distance between the sample and the detector is 13.25 cm. The samples for WAXS tests were 1.5-mm-wide, 10-mm-long strips. The alignment degree of MXene flakes is quantified using Herman's orientation factor (*f*), which is defined by the following formula [2,3]:

$$f = \frac{3}{2}\frac{\int_0^{\pi/2} I(\varphi)\cos^2(\varphi)\sin(\varphi)\,d\varphi}{\int_0^{\pi/2} I(\varphi)\sin(\varphi)\,d\varphi} - \frac{1}{2} \tag{2}$$

Where $I(\varphi)$ is the scattering intensity integrated along the azimuthal direction centered at the (002) signal of MXene films. The numerical values are obtained from a Gauss function that is fitted to the data (Figure S7).

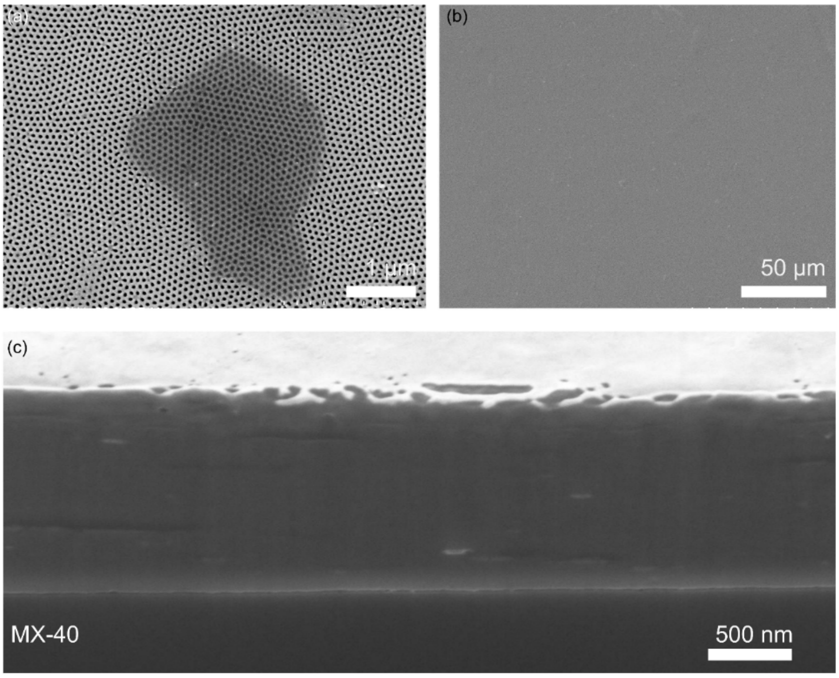

Fig. S1 a SEM image of an MXene flake. **b** SEM image of an MX-80 film. **c** Cross-sectional SEM image of an MX-40 film.

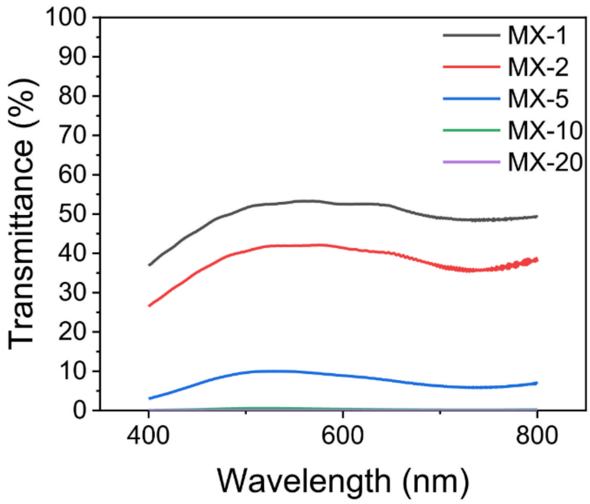

Fig. S2 The light transmittance of the MX-n films with different spraying times.

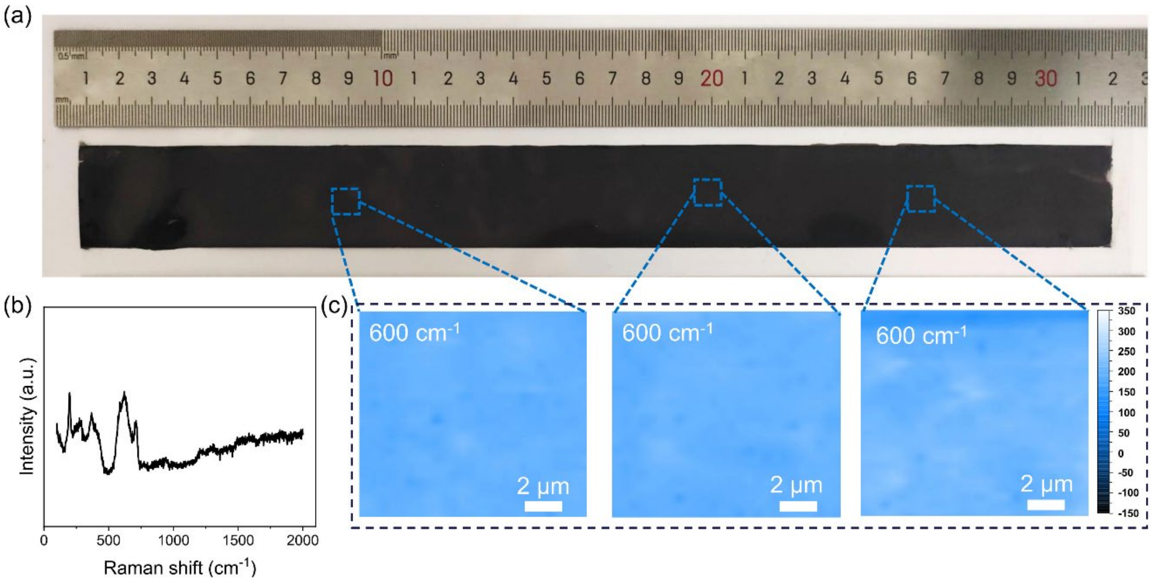

Fig. S3 a The MX-80 film deposited on PET substrate. **b** Raman spectra of the MX-80 film. **c** The Raman mapping of the characteristic mode at different positions of the MX-80 film at 600 cm^{-1}

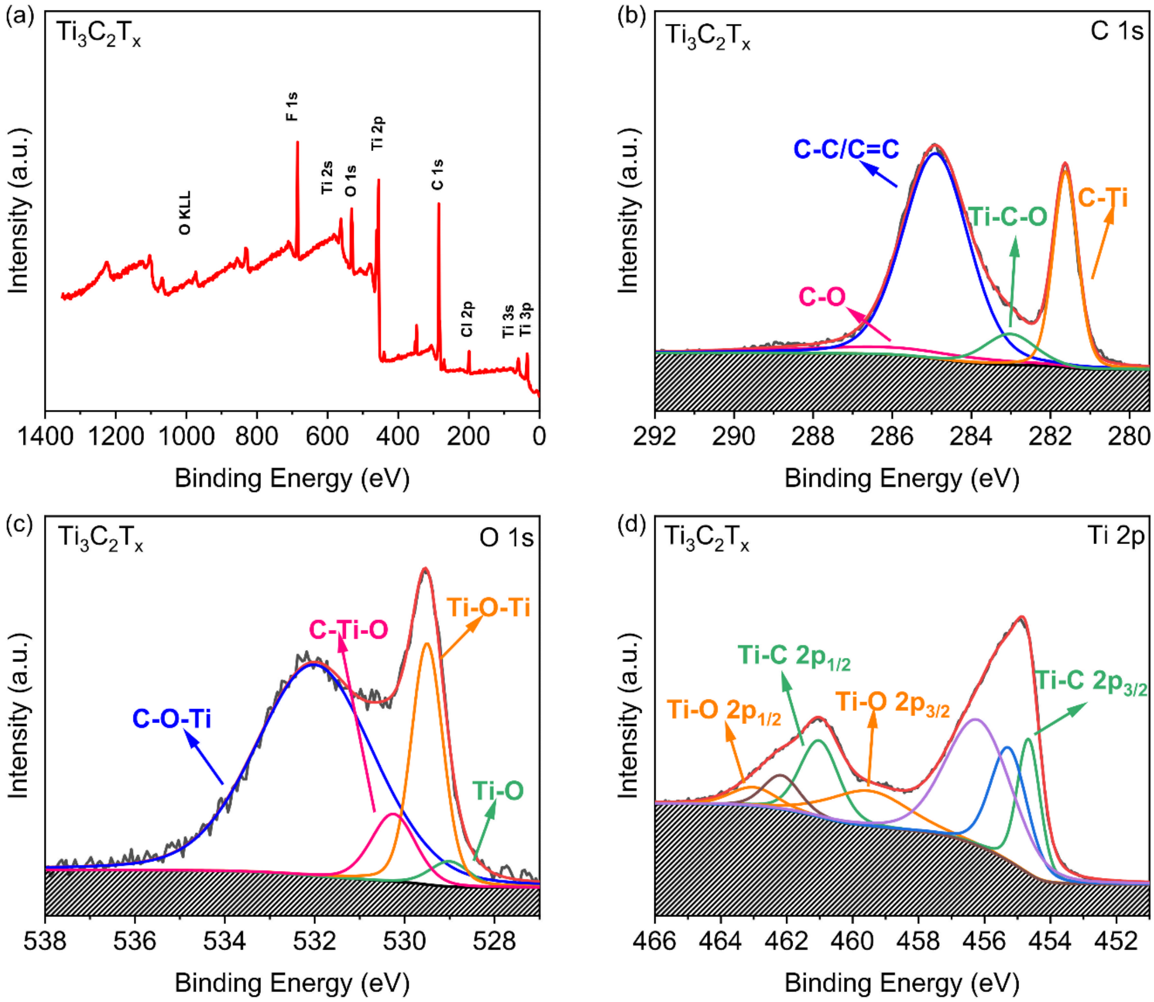

Fig. S4 a XPS spectra of the MX-80 film. **b** C 1s, **c** O 1s, and **d** Ti 2p spectra of the MX-80 film. The XPS results confirm the successful fabrication of $Ti_3C_2T_x$ MXene films [4], with no evidence of significant oxidation.

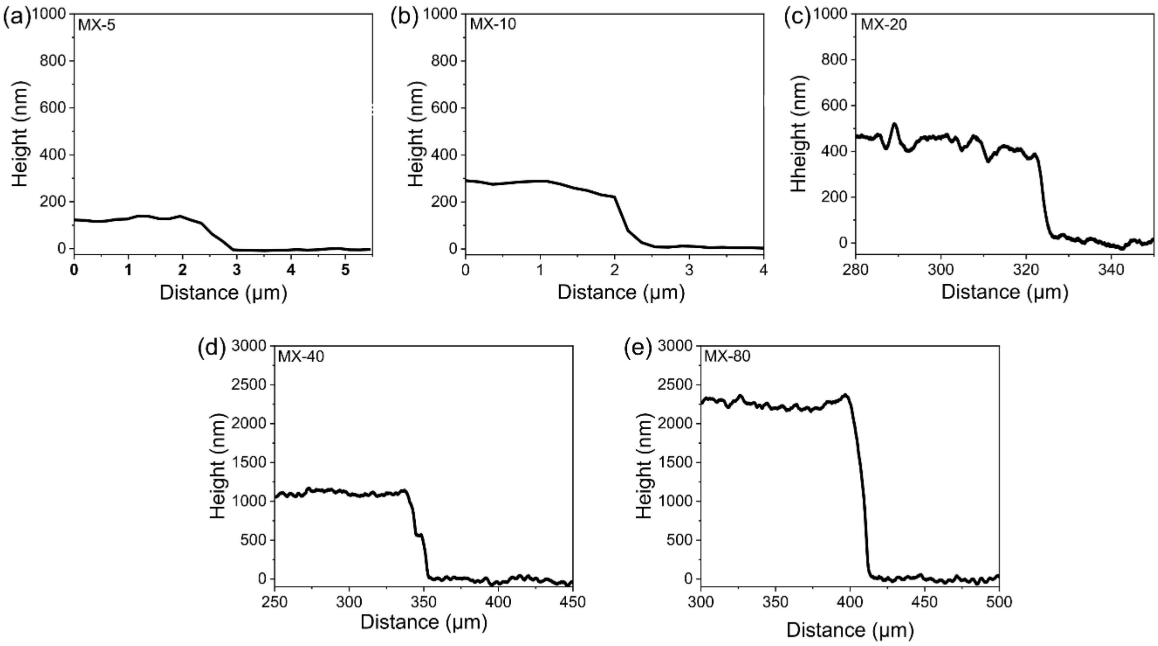

Fig. S5 Thickness distribution of **a** MX-5 film and **b** MX-10 film measured by AFM. Thickness distribution of **c** MX-20 film, **d** MX-40 film, and **e** MX-80 film measured by step profiler.

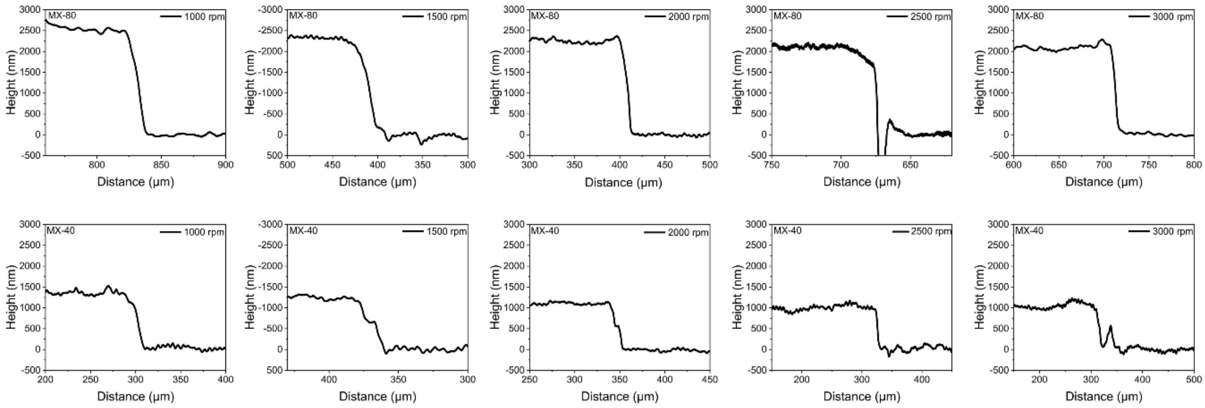

Fig. S6 Thickness distribution of MX-40 films and MX-80 films at different rotating rates measured by step profiler.

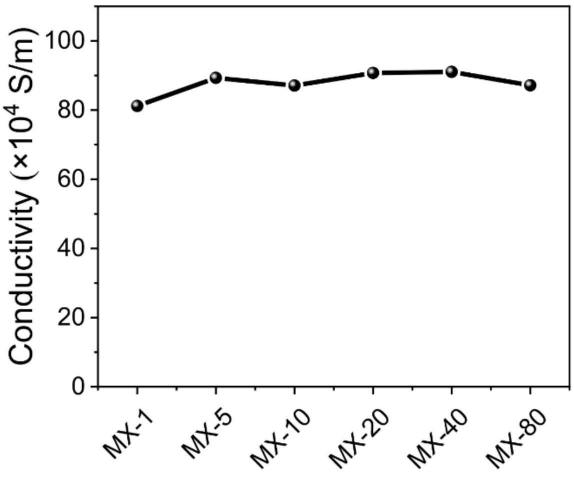

Fig. S7 Conductivity of MX-n films with different spray times.

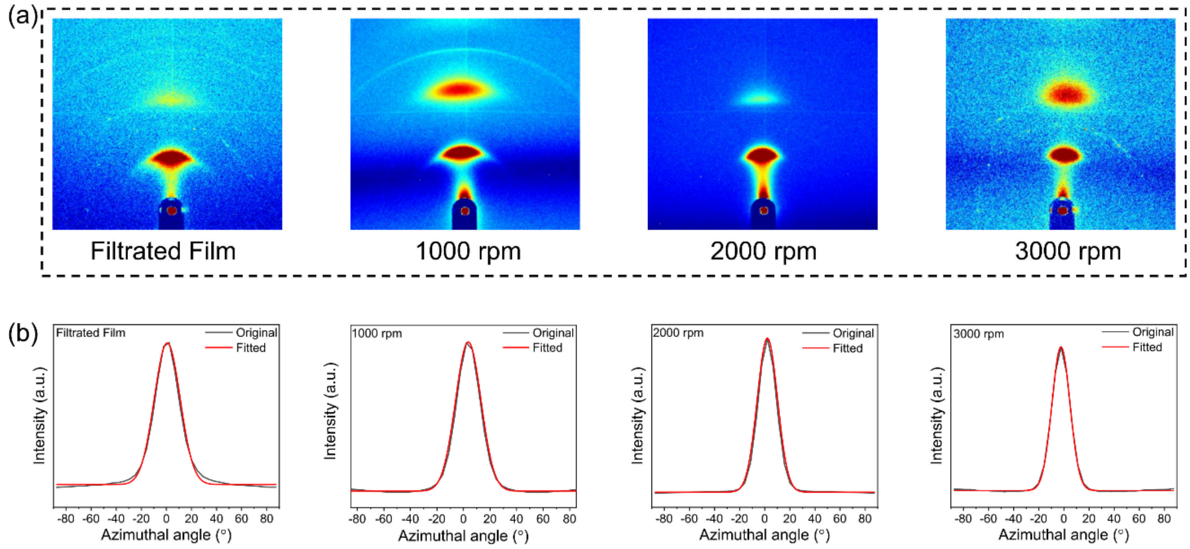

Fig. S8 a WAXS patterns for an incident Cu-Kα X-ray beam parallel to the film plane and **b** **c**orresponding azimuthal scan profiles for the 002 peak for MX-n films and filtrated film.

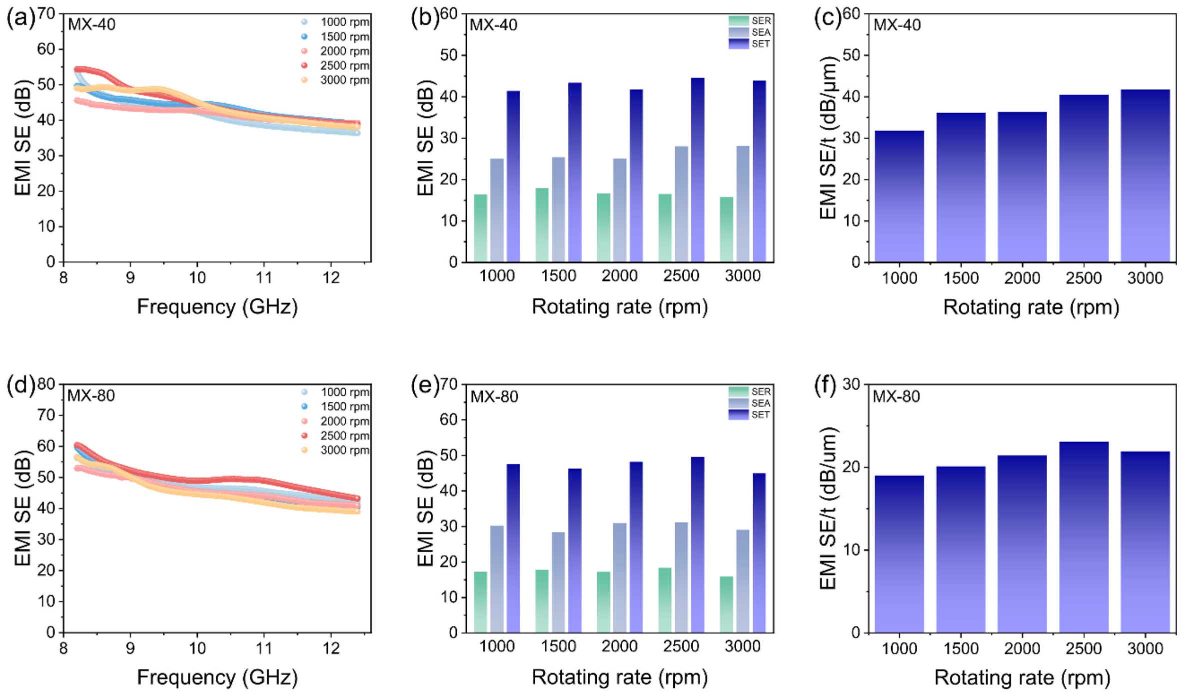

Fig. S9 Total EMI SE of MX-40 films **a** and MX-80 films **d** at different rotating rates in the X-band. Average refection (SE_R), absorption (SE_A), and total EMI SE (SE_T) of the **b** MX-40 films and **e** MX-80 films at different rotating rates in the X-band. EMI SE/t of **c** MX-40 films and **f** MX-80 films at different rotating rates in the X-band.

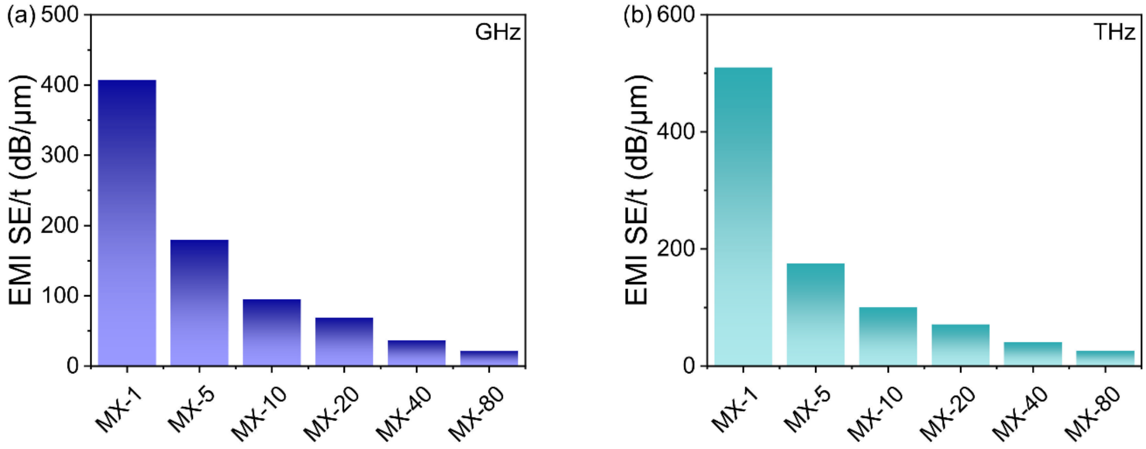

Fig. S10 EMI SE/t of MX-n films with different spraying times in **a** the X-band (8.2-12.4 GHz) and **b** the frequency range of 0.2-1.6 THz.

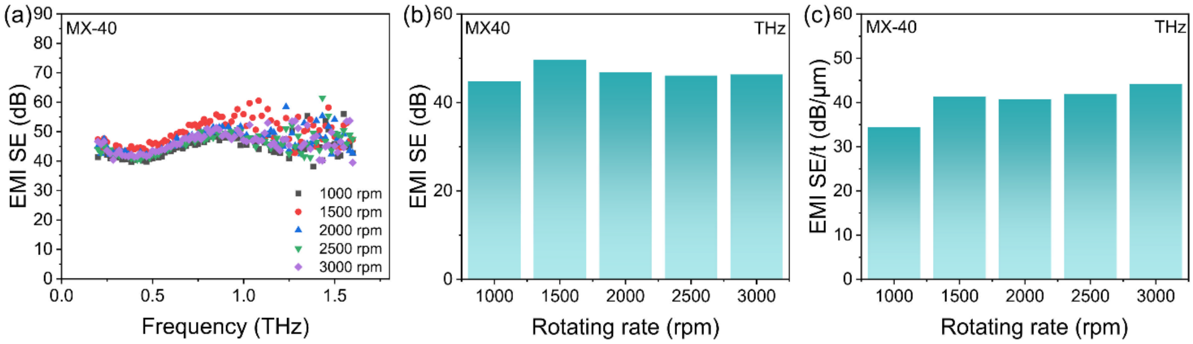

Fig. S11 a Total EMI SE of MX-40 films at different rotating rates in the frequency range of 0.2-1.6 THz. **b** Average EMI SE of the MX-40 films at different rotating rates in the frequency range of 0.2-1.6 THz. **c** EMI SE/t of MX-40 films at different rotating rates in the frequency range of 0.2-1.6 THz.

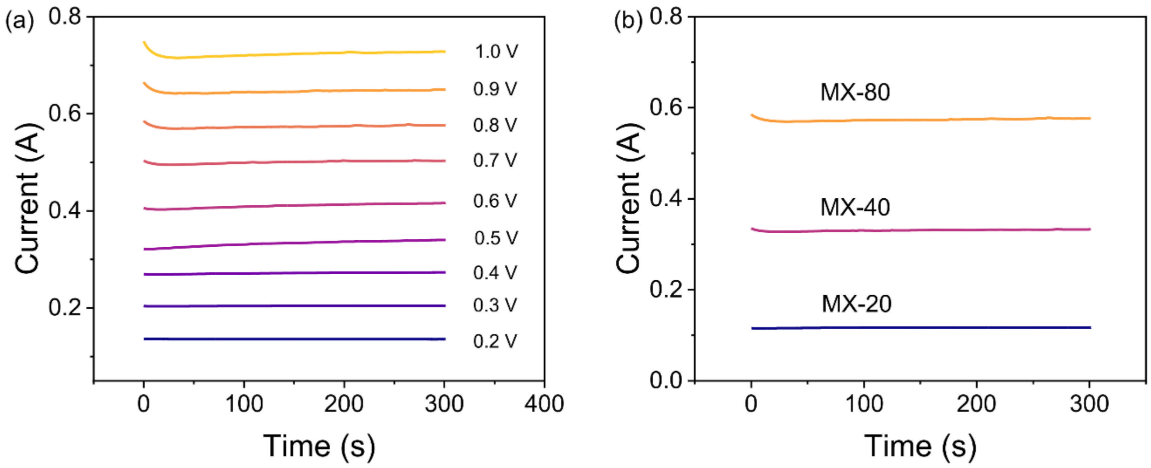

Fig. S12 **a** Corresponding current values of MX-n films at different supplied voltages. **b** Corresponding current values of the MX-n films with different spraying times at 0.8 V supplied voltage.

Table S1 Thickness and SSE/t (defined as the SE divided by thickness and density) of various shielding materials.

Sample	Thickness (μm)	SSE/t ($\times 10^3$ dB $cm^2 g^{-1}$)	Refs.
MXene/CNF Aerogel	1000	26.5	[5]
MXene Foam	6	136	[6]
MXene Fiber	500	48	[7]
MXene Frame	1380	5.1	[8]
MXene/PPy	4	36.9	[9]
MXene/SS/Zn^{2+}	2.52	78	[10]
Graphene/PMMA	0.132	300	[11]
MWCNT	0.6	450	[12]
rGO/BPDD	3.4	53.4	[13]
MXene/PVA/Ag NW	145.4	36.5	[14]
MXene/CNT	0.17	58.2	[15]
Ag NW/PANI	13.3	28.9	[16]
MX-1	**0.025**	**1545**	**This work**
MX-5	**0.14**	**531**	
MX-10	**0.29**	**304**	
MX-20	**0.58**	**216**	
MX-40	**1.15**	**123.5**	
MX-80	**2.25**	**79.5**	

Supplementary References

[1] J. Zhong, W. Sun, Q. Wei, X. Qian, H.-M. Cheng, et al., Efficient and scalable synthesis of highly aligned and compact two-dimensional nanosheet films with record performances. Nat. Commun. **9**, 3484 (2018). https://doi.org/10.1038/s41467-018-05723-2.

[2] H. Park, K. H. Lee, Y. B. Kim, S. B. Ambade, S. H. Noh, et al., Dynamic assembly of liquid crystalline graphene oxide gel fibers for ion transport. Sci. Adv. **4**, eaau2104 (2018). https://doi.org/10.1126/sciadv.aau2104.

[3] X. Hong, Z. Xu, Z.-P. Lv, Z. Lin, M. Ahmadi, et al., High-permittivity solvents increase MXene stability and stacking order enabling ultraefficient terahertz shielding. Adv. Sci. **11**, 2305099 (2024). https://doi.org/10.1002/advs.202305099.

[4] J. Huang, S. Yang, X. Tang, L. Yang, W. Chen, et al., Flexible, transparent, and wafer-scale artificial synapse array based on $TiO_x/Ti_3C_2T_x$ film for neuromorphic computing. Adv. Mater. **35**, 2303737 (2023). https://doi.org/10.1002/adma.202303737.

[5] N. Wu, Y. Yang, C. Wang, Q. Wu, F. Pan, et al., Ultrathin cellulose nanofiber assisted ambient-pressure-dried, ultralight, mechanically robust, multifunctional MXene aerogels. Adv. Mater. **35**, 2207969 (2023). https://doi.org/10.1002/adma.202207969.

[6] J. Liu, H.-B. Zhang, R. Sun, Y. Liu, Z. Liu, et al., Hydrophobic, flexible, and lightweight MXene foams for high-performance electromagnetic-interference shielding. Adv. Mater. **29**, 1702367 (2017). https://doi.org/10.1002/adma.201702367.

[7] T. Zhou, Y. Yu, B. He, Z. Wang, T. Xiong, et al., Ultra-compact MXene fibers by continuous and controllable synergy of interfacial interactions and thermal drawing-

induced stresses. Nat. Commun. **13**, 4564 (2022). https://doi.org/10.1038/s41467-022-32361-6.

[8] X. Wu, T. Tu, Y. Dai, P. Tang, Y. Zhang, et al., Direct ink writing of highly conductive MXene frames for tunable electromagnetic interference shielding and electromagnetic wave-induced thermochromism. Nano-Micro Lett. **13**, 148 (2021). https://doi.org/10.1007/s40820-021-00665-9.

[9] S. Yang, R. Yang, Z. Lin, X. Wang, S. Liu, et al., Ultrathin, flexible, and high-strength polypyrrole/$Ti_3C_2T_x$ film for wide-band gigahertz and terahertz electromagnetic interference shielding. J. Mater. Chem. A **10**, 23570 (2022). https://doi.org/10.1039/D2TA06805B.

[10] S. Wan, Y. Chen, C. Huang, Z. Huang, C. Liang, et al., Scalable ultrastrong MXene films with superior osteogenesis. Nature **634**, 1103 (2024). https://doi.org/10.1038/s41586-024-08067-8.

[11] C. Pavlou, M. G. Pastore Carbone, A. C. Manikas, G. Trakakis, C. Koral, et al., Effective EMI shielding behaviour of thin graphene/PMMA nanolaminates in the THz range. Nat. Commun. **12**, 4655 (2021). https://doi.org/10.1038/s41467-021-24970-4.

[12] H. Wang, X. Sun, Y. Wang, K. Li, J. Wang, et al., Acid enhanced zipping effect to densify MWCNT packing for multifunctional MWCNT films with ultra-high electrical conductivity. Nat. Commun. **14**, 380 (2023). https://doi.org/10.1038/s41467-023-36082-2.

[13] S. Wan, Y. Chen, Y. Wang, G. Li, G. Wang, et al., Ultrastrong graphene films *via* long-chain π-bridging. Matter **1**, 389 (2019). https://doi.org/10.1016/j.matt.2019.04.006.

[14] D. Tao, C. Yang, C. Chen, K. Yan, H. You, et al., Highly flexible and ultralight PVA-co-PE-AgNW/MXene composite film with low filling for multistage electromagnetic interference shielding. Small **21**, 2411752 (2025). https://doi.org/10.1002/smll.202411752.

[15] G.-M. Weng, J. Li, M. Alhabeb, C. Karpovich, H. Wang, et al., Layer-by-layer assembly of cross-functional semi-transparent MXene-carbon nanotubes composite films for next-generation electromagnetic interference shielding. Adv. Funct. Mater. **28**, 1803360 (2018). https://doi.org/10.1002/adfm.201803360.

[16] F. Fang, Y.-Q. Li, H.-M. Xiao, N. Hu & S.-Y. Fu, Layer-structured silver nanowire/polyaniline composite film as a high performance X-band EMI shielding material. J. Mater. Chem. C **4**, 4193 (2016). https://doi.org/10.1039/C5TC04406E.